Article

Neuron

Precise Somatotopic Thalamocortical Axon Guidance Depends on LPA-Mediated PRG-2/Radixin Signaling

Highlights

- PRG-2 at the growth cone mediates axonal LPA sensitivity of thalamocortical fibers
- LPA/PRG-2/RDX signaling in the growth cone is a novel axon guidance mechanism
- PRG-2 deficiency disrupts precision of thalamocotrical somatotopy
- *PRG-2*$^{-/-}$ mice have altered thalamocortical targeting and specific sensory defects

Authors

Jin Cheng, Sadhna Sahani, Torben Johann Hausrat, ..., Matthias Kneussel, Robert Nitsch, Johannes Vogt

Correspondence

robert.nitsch@unimedizin-mainz.de (R.N.), johannes.vogt@unimedizin-mainz.de (J.V.)

In Brief

Cheng et al. describe a new axon guidance mechanism depending on PRG-2 at the growth cone of thalamocortical axons and extracellular LPA synthesized below the cortical plate. Molecular analysis revealed LPA/PRG-2/RDX signaling at the growth cone important for thalamocortical targeting.

Cheng et al., 2016, Neuron *92*, 126–142
October 5, 2016
http://dx.doi.org/10.1016/j.neuron.2016.08.035

CellPress

Neuron
Article

Precise Somatotopic Thalamocortical Axon Guidance Depends on LPA-Mediated PRG-2/Radixin Signaling

Jin Cheng,[1,9] Sadhna Sahani,[1,9] Torben Johann Hausrat,[2,9] Jenq-Wei Yang,[3] Haichao Ji,[1] Nikolai Schmarowski,[1] Heiko Endle,[1] Xinfeng Liu,[1] Yunbo Li,[1] Rahel Böttche,[1] Konstantin Radyushkin,[4] Hans M. Maric,[5] Anna Hoerder-Suabedissen,[6] Zoltán Molnár,[6] Pierre-Hugues Prouvot,[1] Thorsten Trimbuch,[7] Olaf Ninnemann,[7] Jisen Huai,[1] Wei Fan,[1] Barbara Visentin,[8] Roger Sabbadini,[8] Kristian Strømgaard,[5] Albrecht Stroh,[1] Heiko J. Luhmann,[3] Matthias Kneussel,[2] Robert Nitsch,[1,*] and Johannes Vogt[1,10,*]

[1]Institute for Microscopic Anatomy and Neurobiology, University Medical Center, Johannes Gutenberg University, 55131 Mainz, Germany
[2]University Medical Center Hamburg-Eppendorf, Institute for Molecular Neurogenetics, Center for Molecular Neurobiology Hamburg (ZMNH), 20251 Hamburg, Germany
[3]Institute of Physiology, University Medical Center, Johannes Gutenberg University, 55128 Mainz, Germany
[4]Focus Program Translational Neuroscience, Johannes Gutenberg University, 55128 Mainz, Germany
[5]Department of Drug Design and Pharmacology, Center for Biopharmaceuticals, University of Copenhagen, 2100 Copenhagen, Denmark
[6]Department of Physiology, Anatomy, and Genetics, University of Oxford, Oxford OX1 3QX, UK
[7]Institute for Cell Biology and Neurobiology, Charité, 10117 Berlin, Germany
[8]Lpath Inc., San Diego, CA 92121, USA
[9]Co-first author
[10]Lead Contact
*Correspondence: robert.nitsch@unimedizin-mainz.de (R.N.), johannes.vogt@unimedizin-mainz.de (J.V.)
http://dx.doi.org/10.1016/j.neuron.2016.08.035

SUMMARY

Precise connection of thalamic barreloids with their corresponding cortical barrels is critical for processing of vibrissal sensory information. Here, we show that PRG-2, a phospholipid-interacting molecule, is important for thalamocortical axon guidance. Developing thalamocortical fibers both in PRG-2 full knockout (KO) and in thalamus-specific KO mice prematurely entered the cortical plate, eventually innervating non-corresponding barrels. This misrouting relied on lost axonal sensitivity toward lysophosphatidic acid (LPA), which failed to repel PRG-2-deficient thalamocortical fibers. *PRG-2* electroporation in the *PRG-2*$^{-/-}$ thalamus restored the aberrant cortical innervation. We identified radixin as a PRG-2 interaction partner and showed that radixin accumulation in growth cones and its LPA-dependent phosphorylation depend on its binding to specific regions within the C-terminal region of PRG-2. In vivo recordings and whisker-specific behavioral tests demonstrated sensory discrimination deficits in *PRG-2*$^{-/-}$ animals. Our data show that bioactive phospholipids and PRG-2 are critical for guiding thalamic axons to their proper cortical targets.

INTRODUCTION

The thalamocortical projection is essential for sensory processing. In rodents, vibrissae provide input to specific thalamic nuclei and these nuclei have well-defined connections with the somatosensory cortical region where sensory information is processed (Woolsey and Van der Loos, 1970). These connections have a somatotopic organization, and sensory information from each vibrissa reaches a specific barreloid in the thalamic ventrobasal (VB) complex and is relayed to a specific cortical barrel field in the primary somatosensory cortex. During their developmental outgrowth, thalamocortical axons are guided by a variety of cues (Molnár et al., 2012). After crossing the subpallial-pallial border, thalamocortical axons advance within the intermediate zone (IZ) and, approaching the cortex, they accumulate below the cortical plate (CP) at the subplate (Ghosh et al., 1990). The interaction of thalamocortical axons with the subplate is one of the most enigmatic processes in the development of thalamocortical fibers. Even in Reeler or p35 knockout (KO) mice, where the subplate is aberrantly located, thalamocortical axons cross the CP toward the misplaced subplate before connecting to their final targets (Hoerder-Suabedissen and Molnár, 2015). However, the molecular mechanisms that control thalamocortical axon-subplate interaction and ultimately the correct targeting of thalamic projections are largely unknown.

In the developing brain, bioactive phospholipids like lysophosphatidic acid (LPA) play important roles in cortical migration (Fukushima et al., 2000) and neuronal apoptosis (Kingsbury et al., 2003). These effects are mediated by LPA receptors, namely LPA_1-R and LPA_2-R, which are expressed in the developing brain (Kingsbury et al., 2003). LPA is a well-described repellent factor for axons, eventually leading to growth cone (GC) collapse (Campbell and Holt, 2003). However, while in vitro experiments suggested an involvement of LPA_1-R in LPA-mediated axonal retraction, deletion of specific LPA receptors did not lead to significant alterations of fiber tracts in the brain (Contos et al., 2002) and did not affect inhibitory LPA effects on retinal GCs (Birgbauer and Chun, 2010).

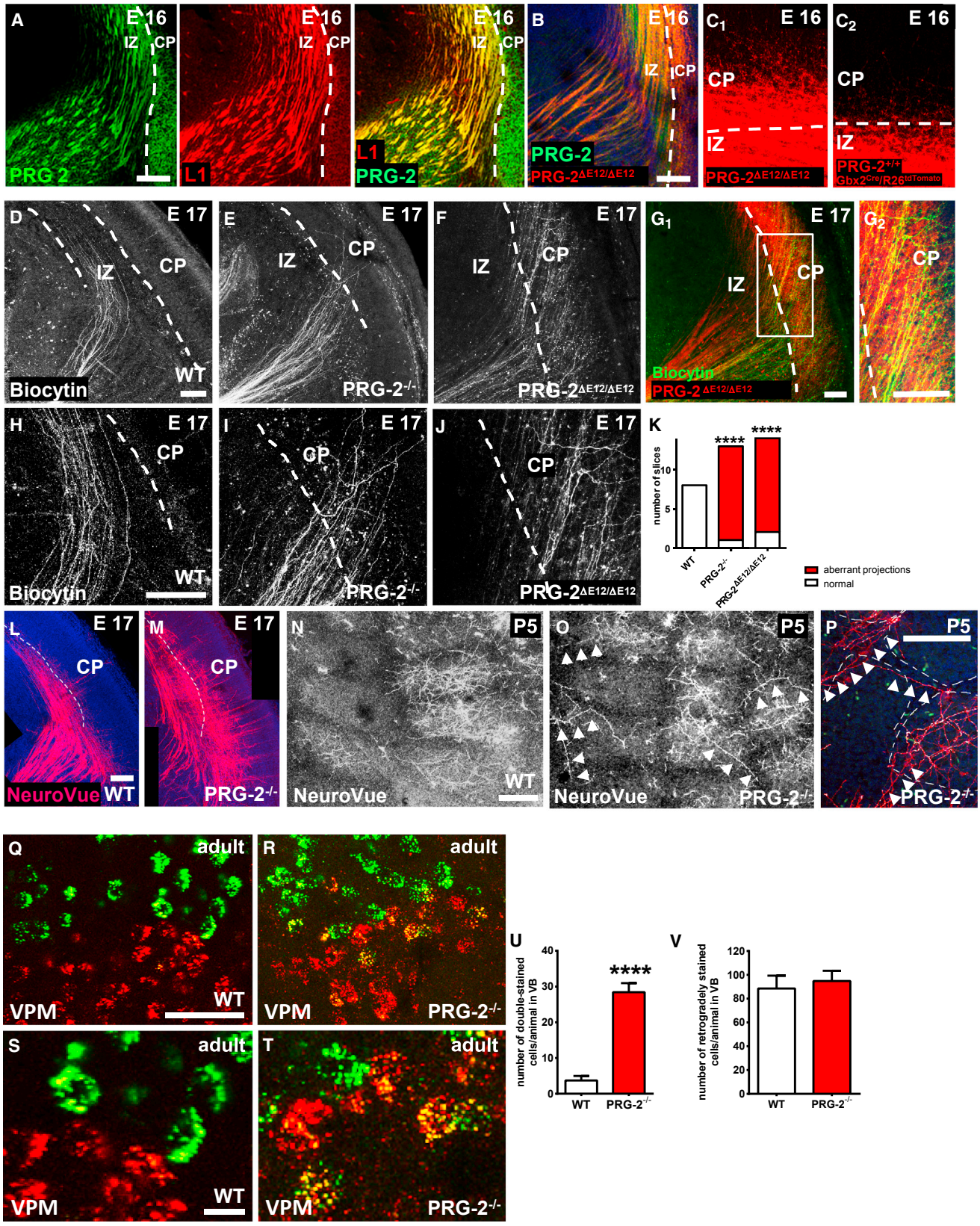

(legend on next page)

Together, this suggests additional LPA-dependent signaling pathways independent of LPA receptors.

LPA is enzymatically inactivated by dephosphorylation via lipid phosphate phosphatases (LPPs), which are cell-surface lipid enzymes and constitute a large family of phosphatidic acid phosphatases (PAP2). Recently, it was shown that LPA signaling at the synapse is controlled by PRG-1/Lppr4 (Trimbuch et al., 2009), which belongs to a new class of LPA-interacting molecules (plasticity-related genes, PRGs) sharing transmembrane features of the LPPs (Bräuer et al., 2003) but which seem to have a different mode of action (McDermott et al., 2004). Among these, PRG-2/Lppr3 is expressed in developing thalamocortical axons and has a high expression level in GCs. Using both *PRG-2*$^{-/-}$ animals and a thalamus-specific PRG-2$^{\Delta E12/\Delta E12}$/Gbx2^{CreER}/R26^{tdTomato} mouse line, we set out to analyze the role of this new LPA regulatory mechanism in outgrowing axons.

RESULTS

PRG-2$^{-/-}$ Mice Have an Aberrant Thalamocortical Projection

PRG-2/Lppr3 is prominently expressed in the thalamus (as shown by in situ hybridization by http://www.genepaint.org; Figure S1B, available online) and in developing thalamocortical fibers (Figures 1A and S1A; for antibody specificity see Figures S1G–S1I), where PRG-2 co-localized with the thalamic axonal marker L1 (Robichaux et al., 2014). According to this expression pattern, we hypothesized that PRG-2 plays a role in the developing thalamocortical projection. We therefore performed biocytin tracing studies in thalamocortical brain slices of wild-type (WT) and *PRG-2*$^{-/-}$ mice at embryonic day (E)17 (Figures 1D, 1E, 1H, and 1I), a time point when thalamocortical axons accumulate below the subplate (Molnár et al., 1998). Slices were injected with Alexa 488-labeled biocytin into the VB complex of the thalamus and were incubated for 6 hr to allow for anterograde biocytin transport. This procedure combines the advantages of maintaining slice integrity with precise tracer application in the VB. While WT thalamocortical fibers were restricted to the IZ (Figures 1D and 1H), as described by others (Molnár et al., 1998), *PRG-2*$^{-/-}$ fibers aberrantly protruded into the CP (Figures 1E and 1I). To further substantiate this finding, we used a conditional PRG-2$^{fl/fl}$ mouse line (Figures S1E and S1F), which was cross-bred with a Gbx2^{CreER} line, resulting in thalamus-specific CreER expression (Chen et al., 2009; Normand et al., 2013), and an R26^{tdTomato} line (Madisen et al., 2010), which produces red fluorescent protein (RFP) upon cre-mediated recombination. Using thalamus-specific PRG-2-deficient mice (PRG-2$^{fl/fl}$/Gbx2^{CreER}/R26^{tdTomato}), we analyzed the effects of thalamus-specific PRG-2 deletion induced by tamoxifen treatment at E12.5 (PRG-2$^{\Delta E12/\Delta E12}$; see also Figures S1C and S1D), as described (Normand et al., 2013). Here, we found a similar aberrant phenotype as observed in constitutive *PRG-2*$^{-/-}$ mice (Figures 1F and 1J). To prove that not only a fiber subpopulation aberrantly protruded into the CP, we analyzed the full thalamocortical projection, which was displayed by the RFP reporter, and confirmed the aberrant phenotype (Figure 1G). Quantitative assessment of these slices revealed a significant disruption of the thalamocortical projection in constitutive *PRG-2*$^{-/-}$ mice as well as in PRG-2$^{\Delta E12/\Delta E12}$ mice (Figure 1K). To demonstrate that misrouting was also present in vivo, we applied NeuroVue tracer in the thalamic VB at E17 in fixed whole brains and analyzed thalamocortical axons. While thalamocortical fibers formed well-defined projections restricted to the IZ in WT animals (Figure 1L), in *PRG-2*$^{-/-}$ mice, thalamocortical fibers invaded the CP, showing a similar misrouting as observed in biocytin-traced thalamocortical slices (Figure 1M). To avoid remote effects, e.g., by PRG-2 deletion in the cortex, we analyzed the thalamocortical projection in vivo in PRG-2$^{\Delta E12/\Delta E12}$ mice, where the RFP reporter delineated the thalamocortical fibers with high accuracy, as described by others (Normand et al., 2013). Here, PRG-2-deficient thalamocortical fibers aberrantly invaded the

Figure 1. PRG-2 Deficiency Alters Thalamocortical Projection

(A) PRG-2 is expressed in thalamocortical fibers and co-localizes with the axonal marker L1 at E16 (see also Figures S1A and S1B).

(B) Thalamus-specific PRG-2 deletion by tamoxifen administration at E12.5 (PRG-2$^{\Delta E12/\Delta E12}$) resulted in aberrant thalamocortical fibers (displayed by the RFP reporter), which prematurely invaded the cortical plate (CP).

(C) Higher magnification of the IZ/CP border shows aberrant thalamic fibers protruding into the CP while WT PRG-2-expressing fibers were restricted to the IZ (C_2).

(D–F and H–J) Thalamocortical fiber tracing using in vivo tracer biocytin injected in the ventrobasal (VB) nuclei of acute thalamocortical slices. While in WT slices (D and H), thalamocortical fibers were restricted to the IZ, in *PRG-2*$^{-/-}$ (E and I) and PRG-2$^{\Delta E12/\Delta E12}$ (F and J) slices, thalamic axons aberrantly invaded the CP.

(G) Using the Cre-driven RFP reporter, the full extent of the thalamic projection in PRG-2$^{\Delta E12/\Delta E12}$ is shown together with biocytin-labeled fibers in the overview (G_1) and at higher magnification (G_2).

(K) Quantitative analysis shows significant amount of aberrant fibers in *PRG-2*$^{-/-}$ and in PRG-2$^{\Delta E12/\Delta E12}$ slices (Fisher's exact test; n = 8 WT, 13 *PRG-2*$^{-/-}$, and 14 PRG-2$^{\Delta E12/\Delta E12}$ slices).

(L and M) Lipophilic dye tracing in E17 fixed brains depicted normal thalamocortical tract in WT animals (L) and high amount of aberrant fibers in *PRG-2*$^{-/-}$ mice (M).

(N–P) Thalamocortical fibers at P5 are restricted to specific barrels in the WT brain (N), while in *PRG-2*$^{-/-}$ brains numerous fibers (arrow heads) crossed barrel borders (O and P; see also Figure S1L).

(Q and R) Following paired injection of fluorescent-labeled retrobeads in different barrels, retrograde-labeled neurons in the thalamic VPM nucleus of WT adult mice show clear segregation (Q; see also Figures S2D–S2G). In contrast, in *PRG-2*$^{-/-}$ mice, numerous double-labeled neurons were found in the thalamic VPM (R).

(S and T) Higher magnification of (Q) and (R).

(U and V) Analysis of double-stained and total number of stained neurons in the thalamic VPM (t test [U] and Mann-Whitney U test [V]; n = 11 WT and 7 *PRG-2*$^{-/-}$ mice). Bars represent mean ± SEM.

****p < 0.0001. Scale bars, 100 (A, B, D–J, and L–P), 50 (Q and R), and 10 μm (S and T).

CP, while PRG-2-expressing fibers were restricted to the IZ (Figures 1B and 1C). Interestingly, in *PRG-2*$^{-/-}$ animals, the subplate had a normal appearance (Figures S1J and S1K) and the cortical organization, as well as the synaptic connectivity, was not altered (Figures S1M–S1T), ruling out possible subplate or cortical defects that could induce mistargeting of thalamocortical fibers (Ghosh et al., 1990).

Since thalamocortical projection defects observed at prenatal stages might be a temporary feature that eventually disappears after formation of thalamocortical connections, we analyzed the thalamocortical fiber tract at postnatal day (P)5, a time point at which the connections of these fibers are established (Molnár et al., 1998). We applied lipophilic tracers in different brain areas (motor cortex, somatosensory cortex, and visual cortex) at P5 and found that retrogradely labeled thalamocortical fibers derived from their corresponding thalamic nuclei grossly maintained their termination pattern (Figures S2A–S2C). To analyze whether the thalamocortical projection to the somatosensory cortex follows the well-established somatotopic termination pattern to the appropriate barrels, we inserted lipophilic tracers in the VB and visualized the thalamic projection in the corresponding barrels in tangential cut cortical slices. As shown in Figure 1N, in the somatosensory cortex of WT animals lipophilic tracer-stained axons were restricted to their corresponding barrels. However, in *PRG-2*$^{-/-}$ mice, thalamic axons readily crossed barrel borders aberrantly invading neighboring barrels (Figures 1O, 1P, and S1L). To further assess misrouting in *PRG-2*$^{-/-}$ mice, we performed retrograde tracing of thalamocortical fibers by paired injection of retrogradely transported fluorescent latex microbeads into adjacent cortical barrels with 400 μm separation between injection sites. As shown by Agmon et al. (1995), even injections placed in close proximity (75–120 μm apart) resulted in segregated neuronal clusters of retrogradely labeled cells in the thalamic VB (Agmon et al., 1995). While in WT animals, even nearby injections of differently labeled fluorescent beads (red and green fluorescence; see Figure S2D) resulted in labeling of distinct subpopulations in the corresponding VB thalamic nuclei (Figures 1Q and 1S), in *PRG-2*$^{-/-}$ mice, injections even at distant sites (see Figure S2E) resulted in double labeling of the corresponding subpopulations (Figures 1R and 1T; exemplarily retrograde stained neurons in the thalamus are shown in Figures S2F and S2G). Quantitative assessment of double-labeled neurons revealed a significantly higher number in *PRG-2*$^{-/-}$ animals, while the total number of retrogradely traced neurons did not differ between genotypes (Figures 1U and 1V). Thus, PRG2 depletion in mice leads to a misrouting in thalamocortical projections.

PRG-2 Function Is Required in Thalamocortical Afferents for Correct Targeting

To test whether the aberrant thalamic projection in *PRG-2*$^{-/-}$ mice results from absence of PRG-2 in thalamocortical axons, we used thalamocortical slice cultures of E15 WT and *PRG-2*$^{-/-}$ mice at the peak of thalamocortical outgrowth. The thalamocortical projection was visualized by co-electroporation of a *GFP*-expressing construct into the thalamic VB at E15.5. After 48 hr, slice cultures were fixed and the axonal projection was analyzed (Figure 2A). In WT slices, thalamocortical fibers were restricted to the IZ (Figure 2B), while *PRG-2*$^{-/-}$ thalamocortical axons aberrantly invaded the CP (Figure 2C). However, when PRG-2 was re-expressed (together with GFP) in thalamocortical axons, these fibers were again restricted to the IZ and did not show obvious differences to WT fibers (Figures 2D and S3A). Quantitative analysis of thalamocortical cultures confirmed the significant amount of aberrant thalamocortical projections and the rescued targeting of these axons after PRG-2 re-expression (Figure 2E). In sum, re-expression of PRG-2 in thalamocortical axons was sufficient to completely abrogate aberrant targeting of the thalamocortical fiber projection in slices from *PRG-2*$^{-/-}$ mice.

LPA Signaling Is Critical for Thalamocortical Axon Guidance in *PRG-2*$^{-/-}$ Mice

Since PRG-2 is a member of the family of LPA-interacting molecules (Trimbuch et al., 2009), we analyzed the presence of autotaxin (ATX, ENPP-2, LysoPLD), the LPA-synthesizing enzyme, in the somatosensory cortex at E16. ATX is expressed by subplate neurons, as has been shown on the mRNA level (Hoerder-Suabedissen et al., 2013), and by a GFP reporter at corresponding age (Figures S4A and S4B). Due to its secreted and diffusible nature, we found strong ATX expression at the lower border of the CP and at the upper border of the IZ (Figure 3A). Here, ATX immunoreactivity overlaps with that of LPA and PRG-2, which was expressed in fasciculated thalamocortical fibers in the IZ (Figures 3B–3D; higher magnification in Figures 3E–3H). These findings are in line with a putative role of ATX/LPA in restricting PRG-2-expressing thalamocortical fibers to the IZ. Moreover, LPA-degrading enzymes like LPP1 and LPP3 are strongly expressed in the IZ (Figures S6N and S6O), which suggests that proper regulation of phospholipids allows thalamocortical axons to occupy a corridor in the IZ, possibly contributing to the fasciculated appearance of the thalamocortical projection. We therefore perturbed phospholipid signaling and analyzed the effect of inhibited LPA synthesis on the correct targeting of thalamocortical axons. We applied a recently characterized ATX blocker (PF8380) (Gierse et al., 2010), which was shown to effectively decrease LPA concentrations (Vogt et al., 2015), to the medium of WT thalamocortical slice cultures and traced thalamocortical fibers using biocytin. After ATX inhibition (0.1 μM), WT thalamocortical fibers aberrantly invaded the CP (Figure 3J), showing a similar phenotype as observed in slices from *PRG-2*$^{-/-}$ mice (Figures 1E and 1I). Quantitative analysis revealed that this phenotype was observed in more than 92% of all PF8380-treated slices (Figure 3L). To further study whether this effect was due to cortical LPA production, PF8380 was locally injected into the CP. Here, inhibition of ATX in the CP was sufficient to induce an aberrant targeting of thalamocortical fibers (Figure 3K). In contrast, PF8380 injection into the thalamus did not significantly alter the thalamocortical targeting, supporting a role for cortical-derived LPA in thalamocortical guidance (Figure 3L). Taken together, our data provide strong evidence that correct guidance of thalamic fibers to the cortex depends on subplate-derived LPA, produced by ATX, and on the presence of PRG-2 on thalamic fibers.

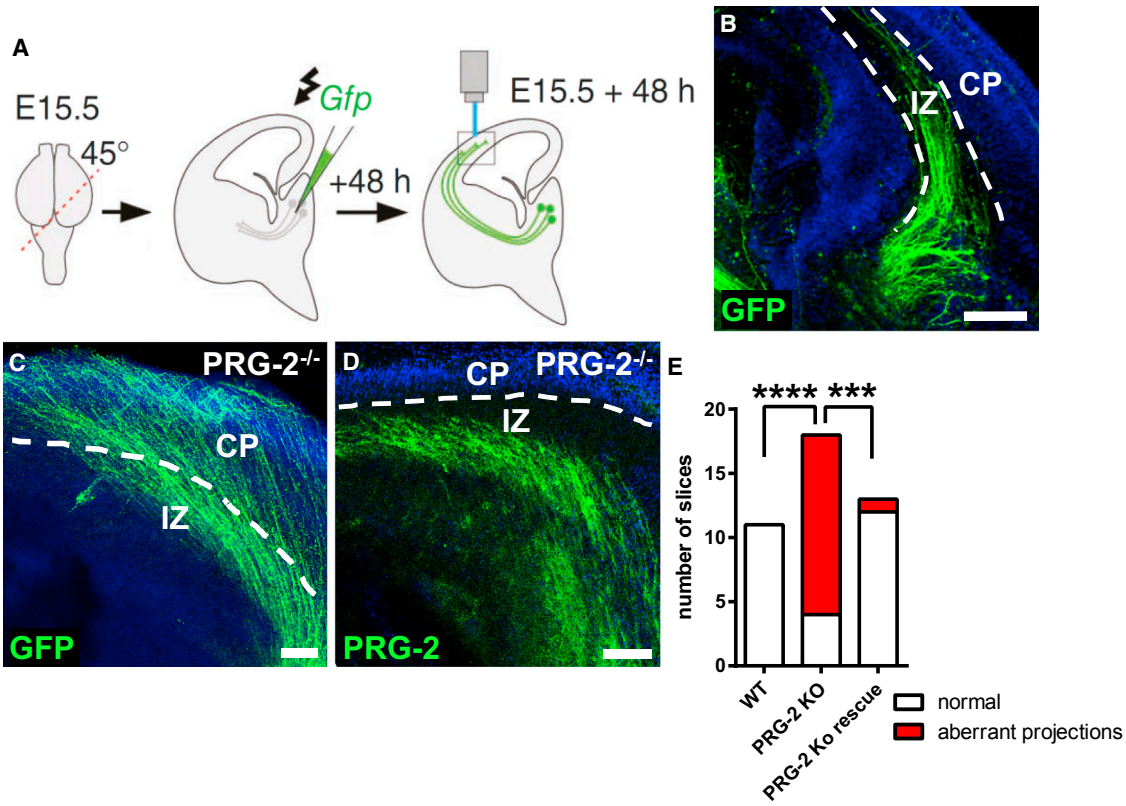

Figure 2. PRG-2 Reconstitution Rescues *PRG-2*$^{-/-}$ Phenotype

(A) Schematic drawing of the thalamocortical slice preparation, *GFP*/*PRG-2* electroporation, and incubation time. Using a cutting angle of 45°, thalamic neurons and their cortical projection region are maintained in a single slice.

(B) WT thalamocortical slice cultures transfected with *GFP* at E15.5 display a typical thalamocortical projection.

(C) In contrast, in *PRG-2*$^{-/-}$ thalamocortical slice cultures, aberrant fibers prematurely entered the CP.

(D) Re-expression of PRG-2 in *PRG-2*$^{-/-}$ slices from the same litter rescued the aberrant phenotype, resulting in a thalamocortical projection confined to the IZ (see also Figure S3A).

(E) Statistical analysis revealed a significant aberrant thalamocortical projection in slices from *PRG-2*$^{-/-}$ mice that was restored to WT levels by PRG-2 re-expression (Fisher's exact test; number of analyzed slices = 11 WT, 18 *PRG-2*$^{-/-}$, and 10 *PRG-2*$^{-/-}$ with PRG-2 re-expression).

***p < 0.001, ****p < 0.0001. Scale bars, 200 (B) and 100 μm (C and D).

PRG-2 Mediates Axonal Sensitivity to LPA

The role of LPA in GC collapse is well described (Campbell and Holt, 2003); however, the molecular mechanism transducing LPA action from the membrane to the cytoskeleton is not well understood. While specific, G protein-coupled LPA receptors were reported not to affect LPA-induced collapse of retinal GCs (Birgbauer and Chun, 2010), authors of the same group showed that downstream inhibition of the G12/13-rho-ROCK pathway was capable of inhibiting LPA-induced retinal GC collapse (Fincher et al., 2014). This is in line with reports of downstream LPA signal transduction acting on the cytoskeleton (Campbell and Holt, 2003). To analyze the role of axonal PRG-2 in LPA-mediated thalamic axon guidance, we embedded thalamic explants in matrigel with a polarized concentration of LPA (distance to TF-LPA-containing matrigel was 401.6 ± 53.63 μm for WT explants and 475 ± 146.80 μm for *PRG-2*$^{-/-}$ explants) and analyzed axonal outgrowth. On one side, the matrigel contained 10 μM fluorescent-labeled LPA (TF-LPA), while the adjacent side did not contain LPA (see Figures 4A, 4B, S5A–S5E, and 4D$_2$ for the border of the TF-LPA-containing matrigel region at higher magnification). The 3D matrigel structure, where fibers are able to radially expand, allows analysis of fiber growth into the LPA-rich zone and the adjacent control zones. However, while WT axons were not able to invade this LPA-rich zone, *PRG-2*$^{-/-}$ axons grew far inside it (Figures 4C and 4D$_1$). Quantitative analysis of fibers entering the LPA-rich zone at different distances revealed significantly higher invasion by fibers from *PRG-2*$^{-/-}$ thalamic slices (Figure 4E), while no difference between WT and *PRG-2*$^{-/-}$ axon fiber outgrowth was observed in the adjacent, non-LPA-containing control side (Figure 4F). Direct comparison of LPA-containing and control sides revealed that WT axons were significantly repelled by the LPA-rich zone, while *PRG-2*$^{-/-}$ axons were not affected (Figure 4G). Since PRG-2 deficiency allowed axons to enter the LPA-rich zone, which is repulsive for WT axons, these data suggest that PRG-2 is critically involved in mediating the repulsive LPA sensitivity in thalamic axons.

During normal development, thalamocortical axons do not collapse at the border to the CP but rather turn away from this

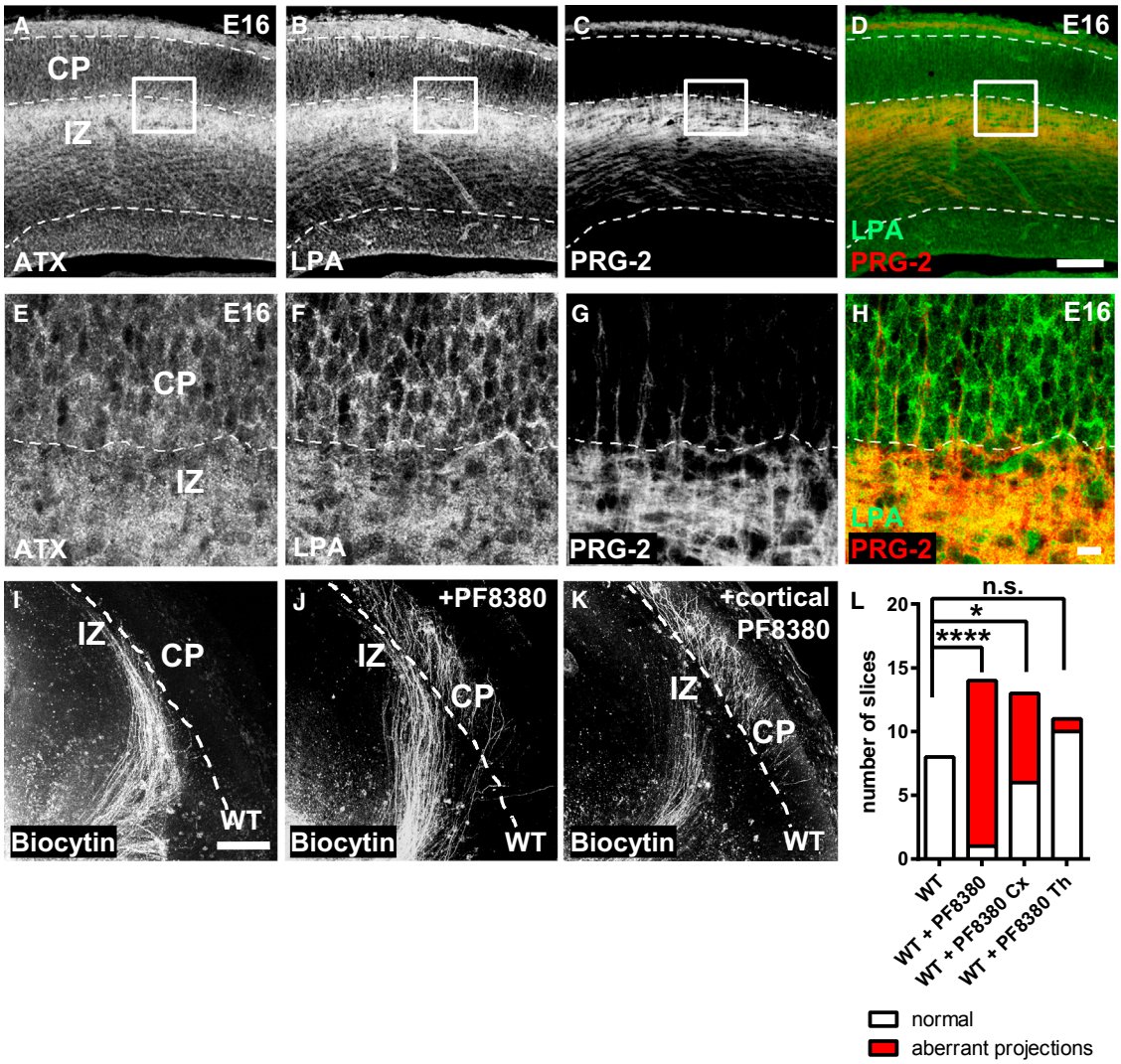

Figure 3. Thalamocortical Fiber Tract Defect in *PRG-2*$^{-/-}$ Mice Is LPA Dependent

(A–D) Autotaxin (ATX; A), the LPA-synthetizing enzyme, and LPA (B and D) are highly expressed in the upper part of the IZ and subplate (see also Figures S4A and S4B). PRG-2-positive fibers are restrained in the IZ (C and D).

(E–H) Higher magnification of the boxed region confirms ATX (E) and LPA (F and H) expression in close proximity to PRG-2-positive thalamocortical fibers (G and H).

(I and J) Biocytine-traced thalamocortical axons develop a normal fiber projection (I), while slices from the same litter incubated with the ATX inhibitor PF8380 (applied to the medium) displayed a severe phenotype with aberrant thalamocortical axons (J).

(K) Cortical injection of PF8380 led to an aberrant thalamocortical fiber projection.

(L) Analysis of aberrant termination of thalamocortical fibers under different conditions revealed significantly disturbed axon guidance after ATX inhibition (Fisher's exact test; number of slices = 8 WT, 14 WT + PF8380 applied to the culture media, 13 WT + cortical PF8380 injection, and 11 WT + thalamic PF8380 injection). *$p < 0.05$, ****$p < 0.0001$. Scale bars, 100 (A–D), 10 (E–H), and 200 μm (I–K).

border and continue to grow in the IZ until reaching their final target. This indicates that LPA provided by the subplate induces the turning of axon GCs when thalamocortical fibers approach LPA-rich areas. To mimic this situation in our in vitro outgrowth assay, we exposed thalamocortical explants to lower LPA concentrations (1 μM LPA; Figure 4H). Here, WT axons displayed a typical turning behavior in front of the LPA-rich zone (Figures 4I and 4K). To confirm this observation, we turned to live imaging of cultured thalamocortical axons. Axon GCs were exposed to a low, but continuous, LPA concentration (500 nM LPA). To avoid bias by perfusion flow, which may repel axons, GCs were exposed to an LPA-covered pipette tip at 40 μm distance (see Figure S5F for experimental overview). While WT axons stopped growing and turned away from the LPA source, this behavior was not observed for *PRG-2*$^{-/-}$ axons, which even seemed to be attracted by LPA (Figures 4L–4N; Movies S1 and S2). Quantitative analysis revealed a significant repulsion of WT axons by 500 nM LPA, which was not observed in *PRG-2*$^{-/-}$ axons (Figure 4O).

However, *PRG-2*$^{-/-}$ axons were still repelled by other guidance cues like Sema3A (Figures S5G and S5H), which are well-described repulsive cues (Mintz et al., 2008). In sum, these data indicate that PRG-2 at the GC mediates the repellent effect of LPA for axonal guidance.

Radixin Is a Downstream PRG-2-Interacting Molecule in the Axon GC

PRG-2/Lppr3 has an intracellular 400 aa-long C-terminal tail, which is putatively involved in signal transduction. To determine interaction partners of this intracellular domain, we first performed a Y2H screen using this PRG-2 C-terminal tail as a bait and found a positive interaction with the FERM domain of radixin (RDX) (Fehon et al., 2010). Using immunoprecipitation (IP) on E17 brain lysate, we confirmed that PRG-2 interacts with RDX (Figures 5A and S6E). This interaction is specific for PRG-2 since only PRG-1 and PRG-2 possess an intracellular C terminus, and PRG-1 is not expressed at embryonic ages (Figure S6J). To further elucidate the role of this interaction in proper guidance of thalamocortical fibers to the developing cortex, we performed co-localization studies at E16 and found co-expression of PRG-2 and RDX in the thalamocortical tract (Figures 5B, 5C, S6K, and S6I). Expression analysis of PRG-2 and RDX showed a similar expression pattern, where expression for both molecules increased from E11.5, a time point where thalamic neurons are already present and start to differentiate (Figure S6F). To prove that the RDX/PRG-2 interaction in fact occurs in the axon GC, we performed subcellular immunofluorescent co-localization studies of RDX and PRG-2 and found a strong signal in GCs (Figure 5D). Here, PRG-2 is expressed at the GC membrane and co-localizes with RDX, which shows an asymmetric distribution, as described by others (Mintz et al., 2008).

RDX belongs to the ezrin, radixin, and moesin (ERM) protein family. However, due to their embryonal expression pattern at E14.5, ezrin and moesin do not seem to be involved in the outgrowth of the thalamocortical projection (Figures S6L and S6M). The C terminus of RDX can directly bind to filamentous actin (F-actin), thereby acting as a crosslinker between the cortical F-actin cytoskeleton and the plasma membrane (Fehon et al., 2010). The activation of RDX involves the phosphorylation of a critical C-terminal threonine residue (T564), which is highly conserved in the ERM protein family. Therefore, we analyzed the role of PRG-2 in RDX activation using a specific antibody that recognizes the phosphorylation of T564 in RDX, T567 in ezrin, and T558 in moesin (Hausrat et al., 2015). Interestingly, we found significantly lower phosphorylated ERM (pERM) levels in *PRG-2*$^{-/-}$ neurons (Figures 5E and 5F), indicating diminished activation of ERM proteins. To prove the role of LPA in ERM activation, we assessed the effect of different LPA concentrations. While 100 nM LPA already revealed an increase in ERM phosphorylation, 1 μM LPA induced a significant and robust increase in pERM levels (Figures 5G and 5H). We further analyzed pERM levels over time and found a fast and constant increase in ERM phosphorylation in the course of LPA stimulation (Figures 5I, 5J, and S6A–S6C). To understand the functional significance of the LPA-dependent pERM expression, we analyzed the RDX/PRG-2 interaction under LPA-free conditions and after 1 μM LPA stimulation for 15 min. Here, we used RDX-GFP transfected, stable PRG-2-expressing HEK cells, which have comparable PRG-2 expression, and performed coIPs of RDX and PRG-2 using an anti PRG-2 antibody (Figure 5K). Quantitative analysis (RDX levels were adjusted according to the PRG-2 IP signal) revealed a significantly increased RDX/PRG-2 interaction upon 1 μM LPA stimulation (Figure 5L). Interestingly, analysis of the IP product revealed that phosphorylation of the PRG-2-interacting RDX was significantly higher upon LPA stimulation when compared to serum-starved cells (Figures 5M and 5N). These data suggest that higher RDX phosphorylation upon LPA stimulation augmented PRG-2/RDX association. Since we could show that RDX binds to the intracellular C terminus of PRG-2 (Figure S6D), to further analyze whether RDX phosphorylation is a prerequisite for PRG-2 binding and to determine the PRG-2 binding sites, we performed a systematic peptide scan using a Celluspot μ Array format (μSPOT) and mapped the RDX/PRG-2 interaction (Figure 5O). Here, PRG-2 intracellular C-terminal overlapping peptides (69 overlapping peptide fragments, 14 aa in length) were analyzed regarding their binding affinity to RDX-GST or to RDX^{T564A}-GST, its non-phosphorylated form. We detected six putative interaction sites that showed significant difference in their binding to RDX-GST or to RDX^{T564A}-GST, pointing to a lower binding affinity of the non-phosphorylated RDX^{T564A}-GST to PRG-2 (see also Figure S6P). We have therefore performed IPs from stable PRG-2-expressing HEK293 cells transfected either with WT *RDX-GFP* (*RDX*^{WT}) or non-phosphorylated *RDX-GFP* (*RDX*^{T564A}) using the described PRG-2 antibody. In line with data from the peptide-microarray-based mapping, although binding of RDX^{T564A} was present at lower levels when compared to RDX^{WT}, PRG-2/RDX^{T564A} binding could be clearly detected (Figures 5P and 5Q). This points to the fact that RDX phosphorylation, although not a prerequisite for RDX/PRG-2 interaction, significantly increases RDX/PRG-2 interaction. To answer the question of whether RDX/PRG-2 association at the membrane is important for LPA-dependent RDX phosphorylation in neurons, we analyzed the effect of LPA stimulation on pERM expression in WT and *PRG-2*$^{-/-}$ neurons. Here, LPA stimulation of WT neurons resulted in a significant increase in pERM levels, while *PRG-2*$^{-/-}$ neurons failed to show any significant change (Figures 5R and 5S). These results point to a yet unknown, but critical role of PRG-2 in LPA-induced RDX activation.

PRG-2 Mediates pERM Increase at GC Membranes Induced by Extracellular LPA

RDX is concentrated below the plasma membrane, a critical position linking transmembrane signaling to the actin cytoskeleton. Since phosphorylation influences RDX activity in connecting the actin-cytoskeleton with the membrane (Fehon et al., 2010), transmembrane signaling events leading to RDX activation are optimally suited to act in extracellular cue mediated axon guidance. We therefore analyzed the effect of extracellular LPA in inducing pERM changes at the GC membrane in WT and *PRG-2*$^{-/-}$ neurons. In WT GCs, pERM was concentrated in a compartment directly adjacent to the GC membrane (Figures 6A and 6B) and strongly increased upon LPA stimulation (Figures 6E, 6F, and 6I). In contrast, no change of pERM was observed in *PRG-2*$^{-/-}$ GCs (Figures 6C, 6D, and 6G–6I). Moreover, direct

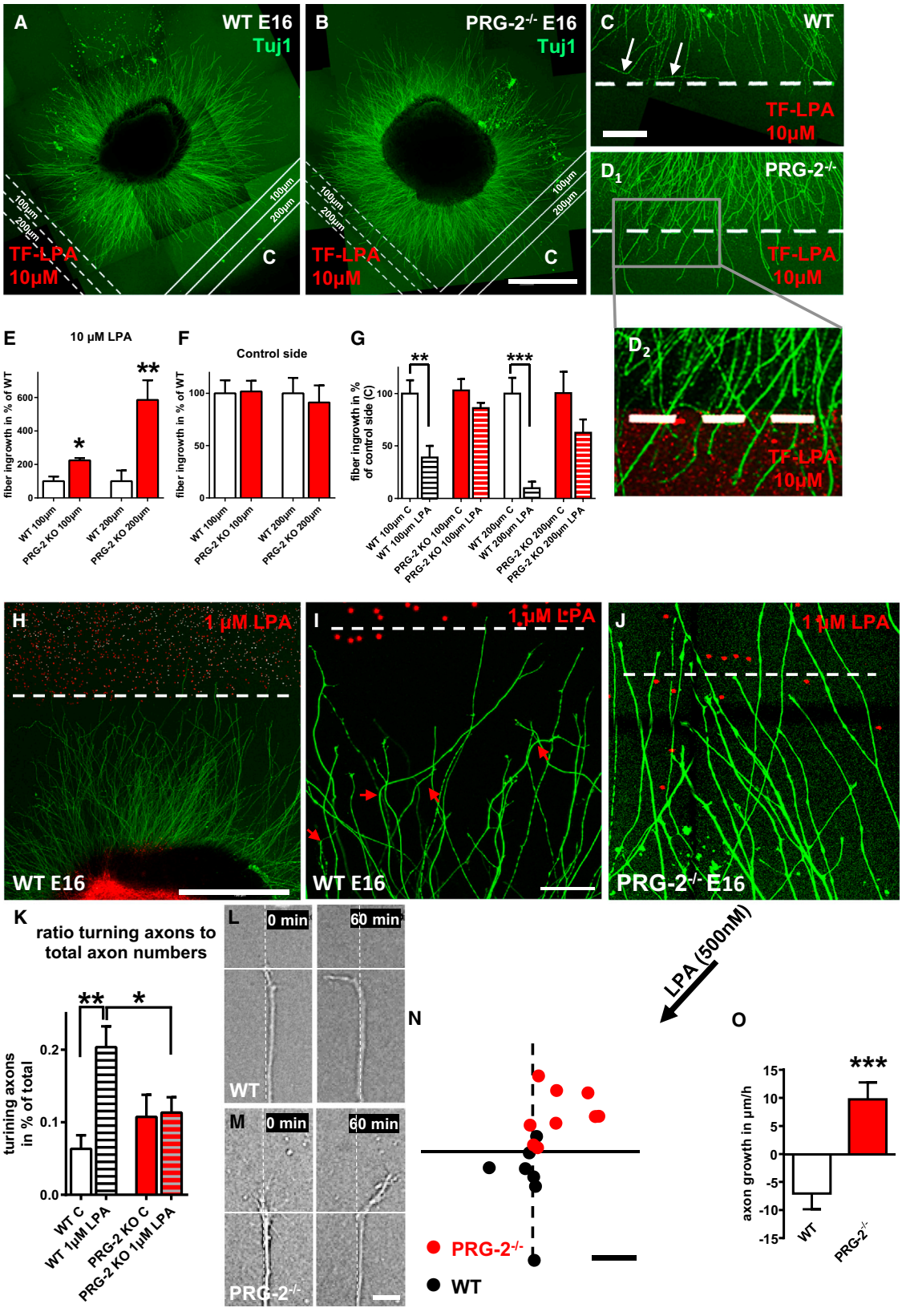

(legend on next page)

comparison of pERM levels in the center of the GC and in the periphery revealed a shift of the pERM signal toward the membrane of WT GCs, but not of *PRG-2*$^{-/-}$ GCs (Figure 6J). To prove whether RDX is dynamically recruited to the membrane via PRG-2 binding induced by a local extracellular LPA source, we transfected WT or *PRG-2*$^{-/-}$ neurons with *GFP*-tagged *RDX* and performed live imaging studies. While in WT neurons, local LPA stimulation rapidly induced a translocation of RDX-GFP to the membrane next to the LPA source (Figures 6K and 6L), *PRG-2*$^{-/-}$ neurons did not show such a change (Figures 6M and 6N). In sum, these data show that PRG-2 is the mediator of LPA-induced localization of RDX to the GC membrane, where it is present in its phosphorylated form, in turn increasing binding to PRG-2.

To prove that ERM phosphorylation and activation play a role in LPA-induced GC turning, we analyzed the subcellular localization of pERM in GCs of thalamic explants exposed to an LPA-rich environment (1 μM LPA), as shown in Figure 4I. Detailed analysis of turning GCs, exemplarily encircled in Figure 7A, revealed strong pERM signal co-localized with F-actin at the tip of GCs turning away from the LPA-rich zone (Figures 7B–7E). To confirm that PRG-2 interacts with RDX at the GC, we performed a proximity ligation assay (PLA), a method that allows the study of in situ protein-protein interactions at resolutions <40 nm (Rhett et al., 2011). Here, we found a strong signal at the GC tip, confirming the PRG-2/RDX interaction at the site of LPA action (Figures 7F and 7G). Taken together, these results confirm the critical role of PRG-2/RDX interaction for the induction of RDX activation in GCs by extracellular LPA, which eventually leads to axon turning.

RDX Deficiency Phenocopies PRG-2 Thalamocortical Axon Defect

To further substantiate the role of RDX in LPA-induced GC turning, we analyzed the thalamocortical projection in *RDX*$^{-/-}$ mice. Using biocytin tracing in living E17 thalamocortical slices, we observed misrouted thalamocortical axons in *RDX*$^{-/-}$ slices that aberrantly invaded the CP (Figures 7I–7K),while in slices from control littermates, the thalamocortical projection was confined to the IZ (Figures 7H and 7K). In order to better understand the functional role of the PRG-2/RDX interaction in thalamocortical axon guidance, we analyzed the effect of partial reduction of these proteins in transheterozygous mice (*PRG-2*$^{+/-}$/*RDX*$^{+/-}$) in thalamocortical slices at E17. Here, the thalamocortical projection aberrantly invaded the CP, suggesting that it is indeed the interaction of PRG-2 and RDX that is important for correct guidance of these fibers by an LPA gradient (Figures 7L–7O). These data corroborate the idea that the LPA-PRG-2-RDX/pERM signal transduction axis is critical for correct guidance and restriction of thalamocortical axons to the IZ. Moreover, in line with decreased RDX expression after E16 (Figures S6G and S6H), these data could explain how thalamocortical axons are finally able to enter into their target cortical region.

Functional and Behavioral Alterations in *PRG-2*$^{-/-}$ Mice

To assess the functional outcome of altered thalamocortical projections in *PRG-2*$^{-/-}$ mice, we first measured intrinsic optical responses in the corresponding barrel upon single-whisker back-and-forth deflection. This approach measures blood-flow changes in the representation of single whiskers in the barrel cortex upon activation. Using this method, we found that the response area upon single-whisker stimulation, which corresponds to the stimulated barrel (for morphological barrel assessment, see Figure S7A), was larger in *PRG-2*$^{-/-}$ mice. These data point to a more diffuse and broader cortical response extending beyond the border of the activated barrel (Figures 8A–8C). Moreover, it reflects our findings using retrograde tracing of thalamocortical fibers in *PRG-2*$^{-/-}$ mice showing a clear overlap in the termination pattern of neurons from neighboring thalamic barreloids in the VPM (Figures 1R, 1T, and 1U). This is in agreement with enlargement of functional barrel columns in mice due to

Figure 4. PRG-2 Deficiency Abolishes Thalamic Axon Sensitivity to LPA

(A and B) Thalamic explants from WT (A) and *PRG-2*$^{-/-}$ (B) mice exposed to 10 μM TF-LPA for 40 hr. TF-LPA-containing zone is located in the lower left part of the image. The opposite, LPA-free right side was regarded as control (C). Lines delineate regions located 100 or 200 μm within the LPA-containing or the control (C) region, respectively. Outgrowing axons stained for Tuj1 were color coded in green.

(C and D) Higher magnification of WT axons at the TF-LPA interface shows a repulsive effect on outgrowing axons (C, arrows). In contrast, *PRG-2*$^{-/-}$ axons were able to enter the LPA-containing region (D_1). Higher magnification shows the border of the TF-LPA-containing region color coded in red (D_2).

(E) Quantitative analysis of fibers protruding 100 and 200 μm into the LPA-rich region (normalized to the number of fibers 100 μm before the TF-LPA-rich matrigel). (Mann-Whitney test; n = 8 WT and 8 *PRG-2*$^{-/-}$ thalamic explants).

(F) On the control side (C; lower right corner in A and B, containing no TF-LPA), no difference was observed when WT and *PRG-2*$^{-/-}$ axons were analyzed at the same distances (as measured to the LPA front). (Mann-Whitney test for 100 μm and t test for 200 μm; n = 8 WT and 9 *PRG-2*$^{-/-}$ thalamic explants).

(G) Comparison of axon numbers at different depths on the LPA-rich side and on the control side. (Kruskal-Wallis test with Dunn's multiple comparisons test; n = 8 WT and 8 *PRG-2*$^{-/-}$ thalamic explants).

(H and I) When exposed to lower LPA concentrations (1 μM; H), thalamic WT axons displayed a turning behavior (I; red arrows pointing to turning axons) in front of the LPA-rich region. Border of the LPA-rich zone is marked by dotted line and visible by addition of red fluorescent beads.

(J) Thalamic explants from *PRG-2*$^{-/-}$ mice at the border of the LPA-rich area displayed no turning behavior and entered the LPA-rich zone in high numbers.

(K) Quantitative analysis of the ratio of turning axons to the total number of axons revealed that WT axons displayed a turning behavior while *PRG-2*$^{-/-}$ axons were not affected by 1 μM LPA (one-way ANOVA with Bonferroni correction for multiple comparisons; n = 8 WT thalamic explants exposed to 1 μm LPA and to control conditions, 11 *PRG-2*$^{-/-}$ thalamic explants exposed to 1 μM LPA, and 8 to control conditions).

(L and M) Live imaging of WT (L) and *PRG-2*$^{-/-}$ GCs (M) exposed to low LPA concentrations (500 nM) at a distance of 40 μm for 60 min (see also Movies S1 and S2; Figure S5F). Line intersection represents GC starting point used for graphic display of axon growth shown in (N).

(N) Schematic diagram showing starting point and end point of GCs during live imaging. Axons extending during live imaging (60 min) into the quadrant facing the LPA source were assigned positive values; axons growing in other quadrants were assigned negative values.

(O) Analysis of GC behavior (unpaired t test; n = 9 WT and 9 *PRG-2*$^{-/-}$ GCs).

*p < 0.05, **p < 0.01, ***p < 0.001. Bars represent mean ± SEM.

Scale bars, 500 (A and B), 100 (C and D_1), 500 (H), 50 (I and J), and 10 μm (L–N).

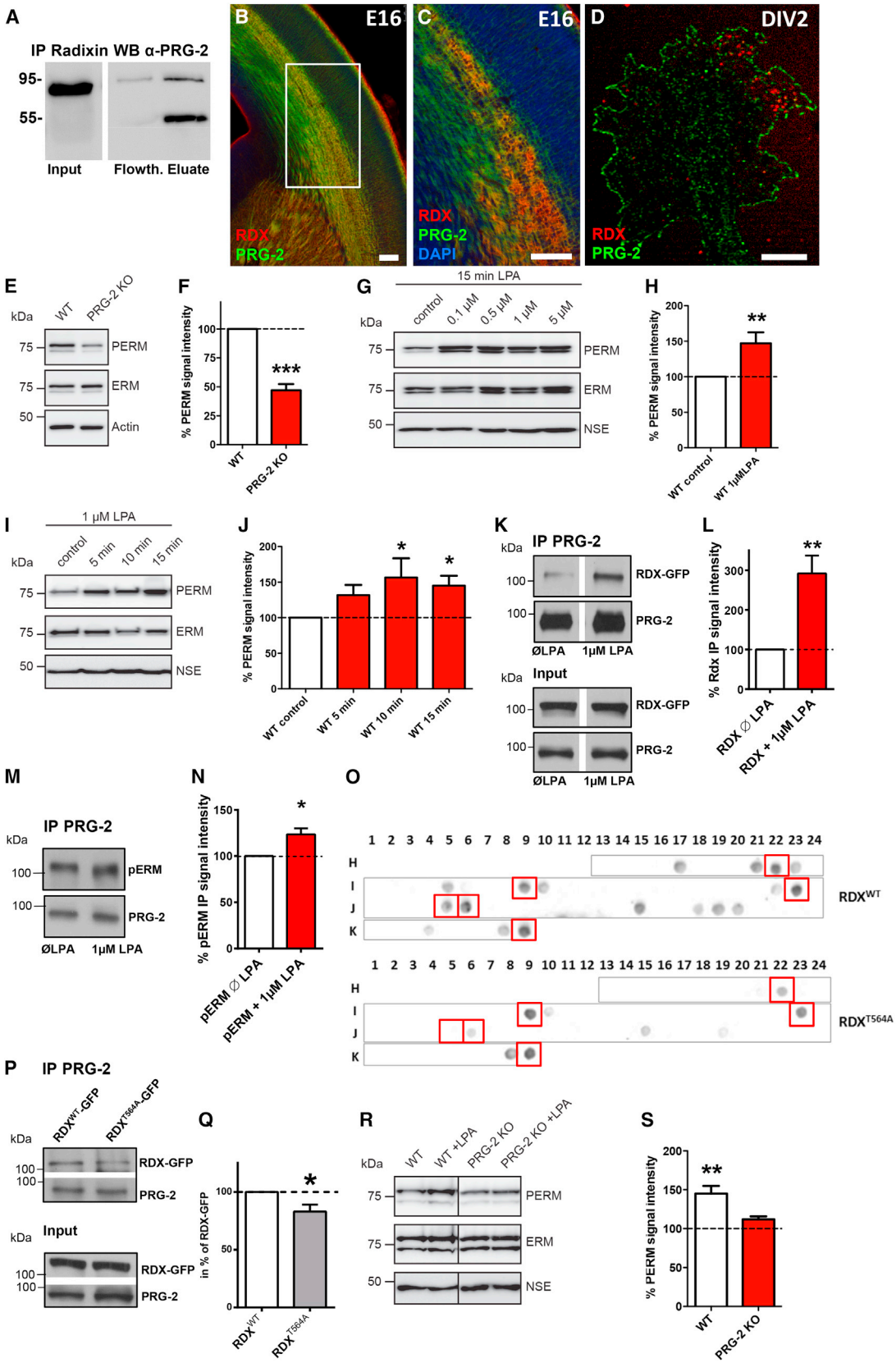

(legend on next page)

impaired precision of the thalamocortical projection, as reported in other mouse models (Lokmane et al., 2013).

To get a layer-specific resolution of neuronal activity, we performed in vivo electrophysiological recordings using multi-channel electrodes. We observed in *PRG-2*$^{-/-}$ mice a slight decrease in multi-unit activity (MUA) upon single-whisker deflection in layer IV and a significant decrease in layers II/III for *PRG-2*$^{-/-}$ mice compared to WT controls (Figures 8D–8F), which are the main target layers of the thalamocortical projection (Meyer et al., 2010). Recent data suggest that layers II/III contain neurons specifically responsive for texture coarseness (Garion et al., 2014). We therefore assessed the ability of *PRG-2*$^{-/-}$ mice to distinguish texture coarseness using a modified radial arm maze, where arms were covered with sandpaper of two slightly different grades (60 grade [grain size, 265 μm] and 80 grade [grain size, 190 μm]; Figure 8G). Only arms covered with the coarser (60 grade) sandpaper were rewarded by accessible food pellets and counted as correct entrance. Since experiments were performed in darkness and no other cues were presented, mice had to orient by sensing sandpaper roughness. While WT mice showed a significant improvement in their ability to choose the correct arm, *PRG-2*$^{-/-}$ mice did not improve beyond chance levels even after 9 days of continuous training (Figure 8H). To exclude bias by an impaired learning ability, we tested *PRG-2*$^{-/-}$ mice in the Morris water maze (MWM). Escape latency for visible and hidden platforms was indistinguishable between *PRG-2*$^{-/-}$ and WT littermates (Figures S7E–S7G). Since learning per se was not impaired in *PRG-2*$^{-/-}$ mice, we conclude that their performance at chance level in the texture discrimination task is a direct result of impaired thalamocortical axon projection precision. In line with unaltered learning ability, motor performance was also unaltered, as shown by analysis in the MWM or supporting limb responses (Figures S7H–S7K). To exclude an effect of PRG-2 deletion outside the thalamus, e.g., in the cortex, which could affect cortical processing of somatosensory information, we also tested the above described thalamus-specific PRG-2-deficient mouse line (PRG-2$^{\Delta E12/\Delta E12}$). As shown in Figures S8L–S8O using retrograde tracing of thalamocortical fibers projecting to the cortical barrels, these animals display a similar phenotype as described for the constitutive *PRG-2*$^{-/-}$ animals, where we could show that different barrels were aberrantly innervated by the same neuron in the thalamic VPM. Furthermore, staining for PRG-2 revealed that fibers originating from Gbx-2-expressing thalamic neurons (identified by the RFP reporter) did not express PRG-2 (Figures S7P–S7S). Behavioral analysis of the PRG-2$^{\Delta E12/\ \Delta E12}$ mice in the sandpaper radial maze revealed that these mice displayed the same phenotype as the constitutive *PRG-2*$^{-/-}$ mice and were not able to distinguish between the two sandpapers of different coarseness (Figure 8H). Together with our in vivo imaging and electrophysiological data, these findings strongly indicate that misguided thalamocortical axons in *PRG-2*$^{-/-}$ mice alter cortical information processing, resulting in a specific deficit in sensory discrimination at adult ages.

DISCUSSION

An intriguing phenomenon in cortical development is the specific outgrowth of thalamocortical fibers that reach the appropriate cortical area before their target cells migrate to their final position in the CP (Kostovic and Rakic, 1990). As shown in other systems, thalamocortical axons accumulate in the IZ below the CP (Ghosh et al., 1990). Here, they interact with a transient neuronal population, the subplate neurons, which keep them in place and are thereby critically important for correct patterning of the thalamocortical connections. Although the role of subplate neurons has long been recognized and gene expression patterns of subplate neurons have been described (for review, see Hoerder-Suabedissen and Molnár, 2015), molecular mechanisms regulating the subplate neurons/thalamocortical fiber interaction are far

Figure 5. PRG-2 Interacts with RDX and Mediates LPA-Dependent pERM Expression in Cortical Neurons

(A) CoIP of RDX and PRG-2 from E17 brain lysates. Antibodies against RDX co-precipitate PRG-2. Signal below PRG-2 band represents heavy chains of the antibody used for IP.

(B) RDX and PRG-2 show clear co-localization along the thalamocortical tract at E16.

(C) Higher magnification of (B).

(D) PRG-2 and RDX are mainly localized at the GC tips.

(E and F) Western blot of *PRG-2*$^{-/-}$ neurons cultivated for 7 days (DIV7; E) shows a lower expression of phosphorylated ERM (pERM) when compared to WT controls (F; one-sample t test; n = 5 cultures per genotype).

(G and H) Western blot (G) and quantification of pERM levels in DIV7 WT neurons stimulated for 15 min with 1 μM LPA (H; one-sample t test; n = 9 cultures per group).

(I and J) Western blot of DIV7 WT neurons stimulated with 1 μM LPA (I) shows significantly increased pERM levels starting 10 min after LPA stimulation (J; one-way ANOVA with Bonferroni correction; n = 18 cultures for 0 and 15 min, n = 9 cultures for 5 and 10 min; see also Figures S6A–S6C).

(K and L) CoIP (using an antibody against PRG-2) of RDX-GFP and PRG-2 after serum starvation of stable PRG-2-expressing HEK cells (K) revealed significantly increased RDX-PRG-2 interaction after 15 min of 1 μM LPA stimulation (L; one-sample t test; n = 6 per group).

(M and N) Western blot of immunoprecipitated RDX-GFP (M; contained in the IP product shown in K) displayed significantly higher pERM levels after LPA stimulation (N; one-sample t test; n = 5 per group).

(O) Peptide-microarray-based mapping of the RDX/PRG-2 interaction in the C-terminal PRG-2 region was assessed for RDX^{WT} and RDX^{T564A}. RDX^{WT} displayed a different binding profile when compared to RDX^{T564A}, as shown for the marked PRG-2 C-terminal cytoplasmic fragments quantitatively analyzed in Figure S6P (see also Table S1).

(P and Q) Western blot (P) and quantitative analysis of IP product from PRG-2-expressing HEK293 cells transfected with RDX^{WT} or RDX^{T564A} (Q; one-sample t test; n = 5 per group).

(R and S) Western blot (R) of *PRG-2*$^{-/-}$ neurons stimulated with LPA (1 μM for 15 min) did not display altered pERM levels (S; one-sample t test; n = 18 WT and n = 7 *PRG-2*$^{-/-}$).

*p < 0.05, **p < 0.01, ***p < 0.001. Bars represent mean ± SEM. Scale bars, 100 (A and B) and 1 μm (D).

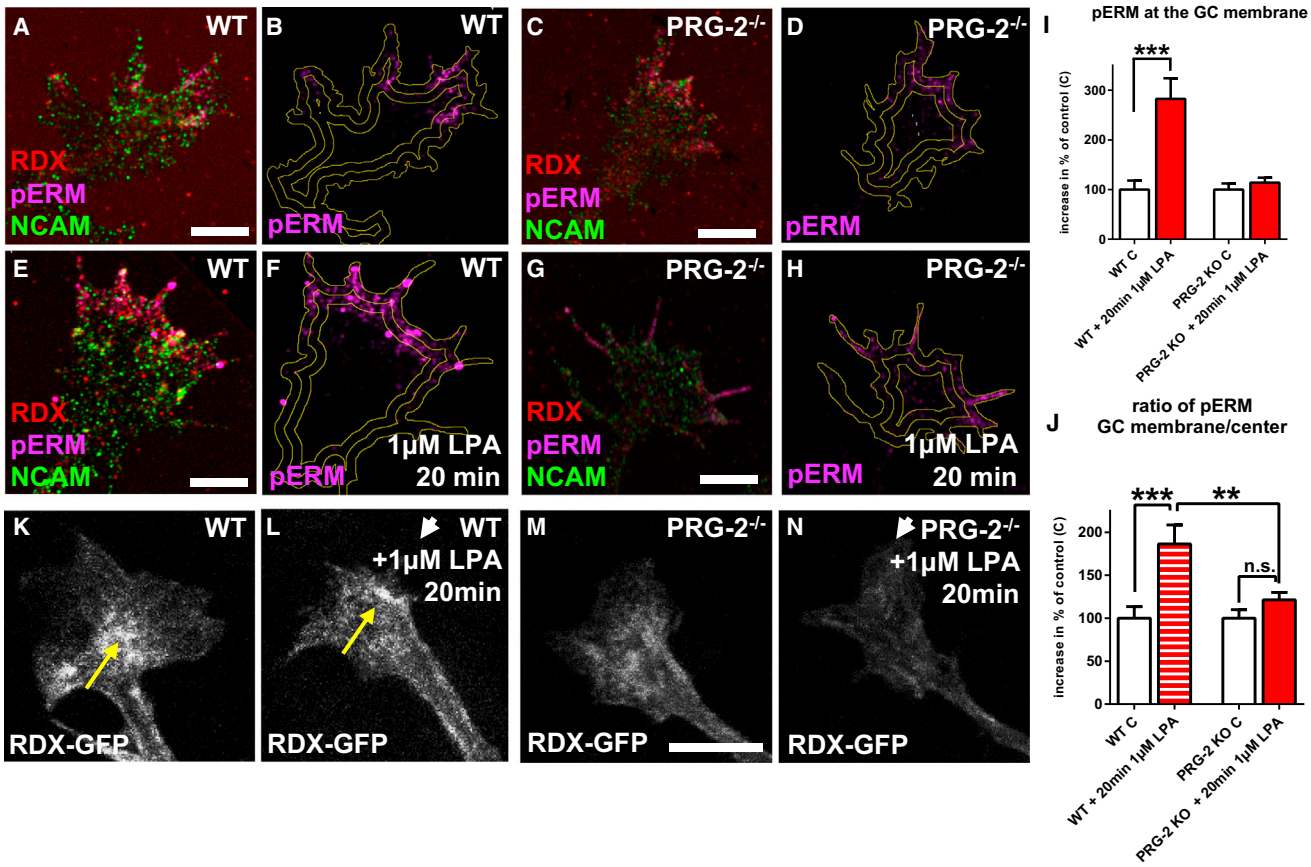

Figure 6. PRG-2 Induces LPA-Dependent pERM Expression at the GC Membrane

(A–D) RDX, pERM, and NCAM expression in a WT (A and B) and in a *PRG-2*$^{-/-}$ GC (C and D) of a DIV2 neuronal culture. Note the prominent pERM expression located at the WT GC membrane (B).

(E–H) LPA stimulation increased pERM expression at the GC membrane in WT axons (E and F), but not in *PRG-2*$^{-/-}$ axons (G and H).

(I) Signal intensity analyses of pERM at the GC membrane upon LPA stimulation (Mann-Whitney test; number of analyzed GCs = 21 non-stimulated and 23 stimulated WT GCs, and 22 non-stimulated and 24 stimulated *PRG-2*$^{-/-}$ GCs).

(J) Ratio of pERM expressed in the GC center and in the periphery significantly increased upon LPA stimulation in WT GCs, while no change was observed in *PRG-2*$^{-/-}$ GCs (one-way ANOVA with Bonferroni correction; number of analyzed GCs = 21 non-stimulated and 20 stimulated WT GCs, and 22 non-stimulated and 24 stimulated *PRG-2*$^{-/-}$ GCs).

(K and L) *RDX-GFP*-transfected GC of a WT neuron at DIV2 before (K) and 20 min after 1 µM LPA stimulation (L). White arrow indicates site of LPA stimulation (500 µM LPA at a distance of 40 µm); yellow arrow indicates RDX-GFP translocation from the GC center to the GC periphery at the site of the LPA application.

(M and N) RDX-GFP distribution in a *PRG-2*$^{-/-}$ neuron at DIV2 before (M) and after LPA stimulation (N) did not markedly change.

**$p < 0.01$, ***$p < 0.0001$. Bars represent mean ± SEM. Scale bars, 5 µm.

from being understood. Here, we analyzed the role of PRG-2/Lppr3, a phospholipid-interacting molecule strongly expressed in thalamocortical axons during development (Figure 1A). Using a constitutive *PRG-2*$^{-/-}$ mouse line as well as a thalamus-specific PRG-2 KO line (PRG-2$^{fl/fl}$/Gbx2^{CreER}/R26^{tdTomato}), where tamoxifen application at E12.5 leads to specific deletion of PRG-2 in the thalamus (PRG-2$^{\Delta E12/\Delta E12}$; Normand et al., 2013), we discovered that PRG-2-deficient thalamocortical axons prematurely and aberrantly entered the CP. This altered the precise somatotopic termination of thalamocortical fibers in the somatosensory barrel field cortex and led to a deficit in sensory discrimination. Molecular analysis revealed a signal transduction axis in the GC leading from the LPA-synthesizing molecule ATX to LPA, PRG-2, and finally to phosphorylated RDX, a well-described linker between the GC membrane and the actin cytoskeleton. We demonstrate this ATX/LPA/PRG-2/pRDX signaling axis on thalamocortical axon GC turning and suggest that this mechanism is responsible for keeping thalamocortical axons in the IZ before entering the CP.

Role of Phospholipids in Subplate/Thalamocortical Axon Interaction

The role of subplate cells was concluded from ablation experiments, where thalamocortical fibers, no longer able to contact subplate cells, escaped the subcortical waiting period and extended beyond their target cortical regions. Here, we found that *PRG-2*$^{-/-}$ thalamocortical axons lose their guidance by the subplate. This specific phenotype relies mechanistically on

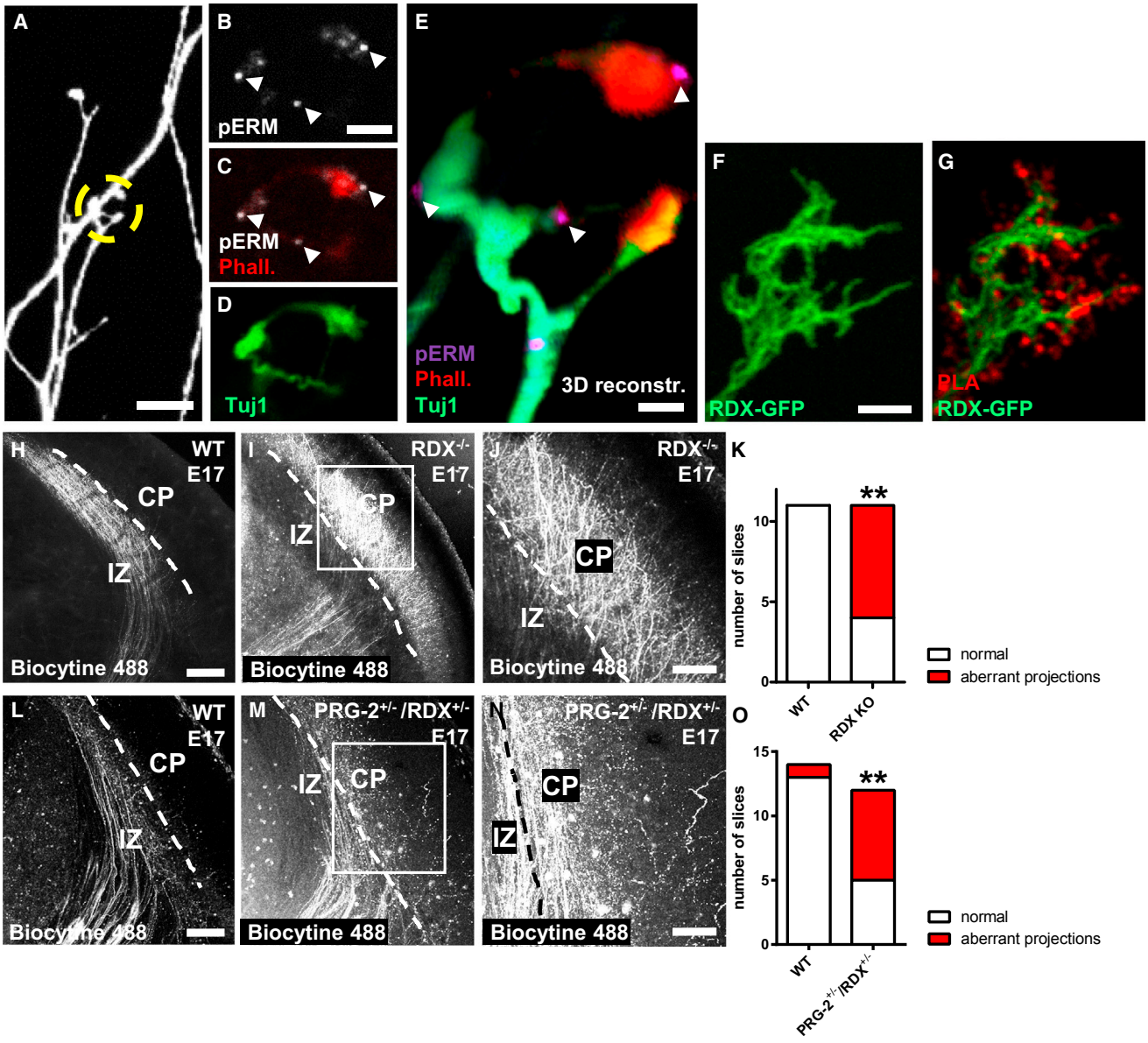

Figure 7. *RDX*$^{-/-}$ Phenocopies *PRG-2*$^{-/-}$ Thalamocortical Defect

(A) Thalamic WT axons growing toward an LPA-containing (1 μM) environment as shown in Figures 4H and 4I.

(B–D) Higher magnification of a Tuj1-positive turning GC (D) highlighted in (A) shows clear pERM expression at the GC tip (B; arrow heads), which contains high amounts of F-actin (C; depicted by Phalloidin in red).

(E) 3D reconstruction of the turning GC shown in (B)–(D). Arrowheads point to pERM expression.

(F and G) Proximity ligation assay (PLA) for PRG-2 and RDX-GFP (F) shows co-localization of PRG-2 and RDX at the GC tip of a DIV2 neuron (G).

(H–K) Biocytin tracing revealed normal distributed thalamocortical fibers in WT slices (H) but an aberrant projection in *RDX*$^{-/-}$ slices (I). Higher magnification of aberrant fibers is shown in (J). Quantitative analysis is shown in (K) (Fisher's exact test; n = 11 WT and 11 *RDX*$^{-/-}$ slices).

(L–O) Biocytine tracing in thalamocortical slices from WT (L) and *PRG-2*$^{+/-}$/*RDX*$^{+/-}$ animals (M and N) at E17 shows an altered thalamocortical projection in *PRG-2*$^{+/-}$/*RDX*$^{+/-}$ slices. Quantitative analysis is shown in (O). (Fisher's exact test; n = 14 WT and 12 *PRG-2*$^{+/-}$/*RDX*$^{+/-}$ slices).

**p < 0.01. Scale bars, 10 (A), 2.5 (B–D), 1.5 (D), 1 (F and G), 200 (H, I, L, and M), and 100 μm (N and J).

the lost sensitivity of thalamocortical axons toward extracellular LPA gradients synthesized by ATX, a diffusible molecule expressed in subplate neurons (Hoerder-Suabedissen et al., 2013). Eventually, this leads to loss of proper axon guidance and to an invasion of inappropriate cortical compartments. Since we also analyzed thalamus-specific PRG-2$^{\Delta E12/\Delta E12}$ KO animals (Normand et al., 2013), we could rule out that this misrouting is due to defects, e.g., derived from cortical PRG-2 deficiency. Interestingly, the same phenotype was detected when the catalytic function of ATX was blocked, thereby impeding LPA

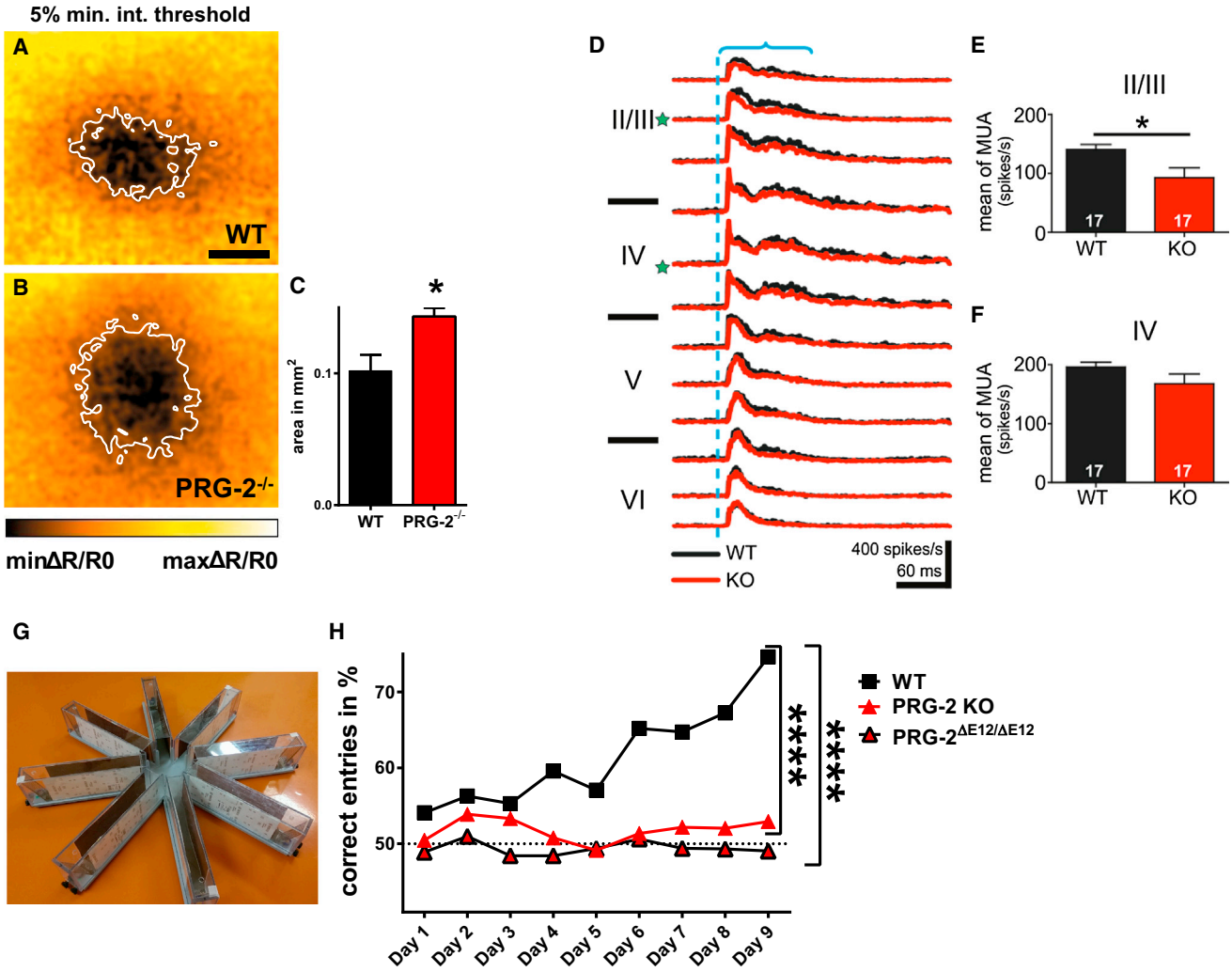

Figure 8. *PRG-2*$^{-/-}$ Mice Have Altered Somatosensory Cortical Processing and a Deficit in Somatosensory Discrimination

(A and B) Color-coded images represent changes in reflection of hemodynamic response (ΔR/R0) after single-whisker stimulation using intrinsic optical imaging (see also Figures S7C and S7D) in WT (A) and *PRG-2*$^{-/-}$ animals (B). Threshold set at 5% ΔR/R0 reflecting steepest drop of hemodynamic response is delineated. High hemodynamic response to single-whisker stimulation in WT animals (A) typically corresponds to one barrel with a sharp delineation toward the neighboring barrels.

(C) *PRG-2*$^{-/-}$ mice revealed a significantly broader hemodynamic response (Mann-Whitney test; n = 7 mice per group). *p < 0.05 at 5% threshold.

(D) Averaged traces of evoked multi-unit activity (MUA) responses recorded in six WT (black trace) and six *PRG-2*$^{-/-}$ (red trace) mice. Blue dashed line indicates time point of whisker deflection and blue braces indicate period from 0 to 100 ms after whisker deflection used for calculation of MUA shown in (E) and (F).

(E and F) MUA in layers II/III (E) and layer IV (F), both marked with green star in (D). Unpaired t test; n = 17 barrel columns from 6 animals per genotype).

(G) Image of the eight-arm maze designed for somatosensory perception where arms are covered with sandpaper of different grain sizes.

(H) Constitutive *PRG-2*$^{-/-}$ mice and thalamus-specific PRG-2-deficient mice (PRG-2$^{\Delta E12/\Delta E12}$) show significant differences in correct performance when compared to WT mice (two-way ANOVA [genotype, time]; n = 8 WT, 20 *PRG-2*$^{-/-}$, and 11 PRG-2$^{\Delta E12/\Delta E12}$ animals).

*p < 0.05, ****p < 0.0001. Bars represent mean ± SEM. Scale bar, 200 μm (A).

production. Our data suggest a thalamocortical guidance mechanism with a mutual dependence on LPA/PRG-2 interaction.

RDX, an F-Actin-Interacting Molecule, Is the Downstream Executer of LPA/PRG-2-Dependent Axon Guidance

The critical importance of PRG-2-mediated extracellular LPA effects on thalamic axon guidance was further clarified by single-axon analysis. While downstream mechanisms mediating LPA GC collapse have been described (Campbell and Holt, 2003), direct and specific LPA-interacting molecules involved in this mechanism remain unclear. In line with live imaging data, WT axons were repelled/collapsed when in contact with 10 μM LPA, while lower LPA concentrations (1 μM) induced a turning behavior in GCs. However, *PRG-2*$^{-/-}$ axons were not affected even by high LPA concentrations (10 μM). Searching for downstream interacting partners, we found RDX to directly interact and be co-expressed with PRG-2 in thalamocortical axons.

Moreover, subcellular analyses revealed RDX to interact with PRG-2 in GCs as shown by PLA. Importantly, IP experiments revealed that the PRG-2/RDX binding was highly increased upon LPA stimulation. The role of this PRG-2/RDX interaction was functionally confirmed, showing that PRG-2 is critically important for RDX activation by extracellular LPA. While in WT neurons, concentrations as low as 100 nM LPA induced clear RDX phosphorylation, in *PRG-2*$^{-/-}$ neurons, RDX phosphorylation did not increase, even upon 15 min of 1 μM LPA stimulation. Our data showing RDX phosphorylation upon LPA stimulation in full-length PRG-2-expressing HEK293 cells suggest that PRG-2/RDX association increased RDX phosphorylation upon LPA stimulation. However, when analyzing binding to PRG-2 to either WT RDX-GFP or its non-phosphorylated form (RDX^{T564A}-GFP), we detected binding under both conditions, albeit with a significant reduction of binding to PRG-2 of the non-phosphorylated form. These data show that RDX phosphorylation is not a prerequisite for PRG-2/RDX binding; however, it influences this binding.

Our finding that transheterozygous loss of PRG-2 and RDX already results in altered thalamocortical fiber projection indicates an important role of the LPA/PRG-2/RDX signal axis. Since the active form of ERMs (pERM) is critical for GC guidance (Mintz et al., 2008), we investigated the role of this signal axis at the GC, the critical location for axon guidance. Here, LPA stimulation induced strong ERM phosphorylation at the GC membrane of WT axons, while *PRG-2*$^{-/-}$ GCs failed to show these changes. In line, RDX was rapidly translocated to the membrane directly next to a local LPA source, indicating an active role of LPA/PRG-2/RDX signaling in GC guidance. Together with the detection of pERM adjacent to F-actin at the tip of turning GCs, this signaling axis appears to directly control LPA-induced axon turning.

In Vivo Effects of Altered Thalamocortical Guidance in Adult *PRG-2*$^{-/-}$ Mice

Using in vivo imaging and high-density multi-electrode recordings in the barrel cortex of *PRG-2*$^{-/-}$ mice and performing behavioral tests both in *PRG-2*$^{-/-}$ mice and PRG-2$^{\Delta E12/\Delta E12}$ animals, we elucidated the functional consequences of PRG-2 deficiency and subsequent altered thalamocortical connectivity in cortical layers IV and II/III as well as in the characteristic discrimination abilities associated with these layers (Garion et al., 2014). It appears that rather specific deficits can be observed even upon drastic developmental defects resulting in grossly impaired cortical lamination and subsequent changes in the thalamocortical projection (Wagener et al., 2016), as shown by preserved functional sensory maps in the somatosensory barrel cortex observed in Reelin-deficient mice (Guy et al., 2015). Interestingly, Cossell et al. (2015) suggest microcircuits in layers II/III are important for specific stimulus orientation (Cossell et al., 2015), supporting the idea that layer II/III neurons mediate rather specific functions. This implies that functional changes in layers II/III seen in *PRG-2*$^{-/-}$ mice can best explain the sensory discrimination deficits of the animal.

Taken together, we describe a novel molecular guidance mechanism involving phospholipid signaling influencing thalamocortial axon guidance at a critical time point, at which axons exhibit a waiting period at the cortical subplate. The alteration of the LPA/PRG-2/pRDX signal transduction pathway resulted in distinct electrophysiological and behavioral deficits in adult animals and highlighted the importance of this pathway for proper thalamocortical connectivity.

EXPERIMENTAL PROCEDURES

Mouse Lines

All experiments were conducted in accordance with the national laws for the use of animals in research and with the European Communities Council Directive 86/609/EEC, and approved by the local ethical committee (Landesuntersuchungsamt Rheinland-Pfalz 23. 177-07/G 13-1-073). Details of the generation and breeding of *PRG-2*$^{-/-}$, PRG-2$^{\Delta E12/\Delta E12}$/Gbx2^{CreER}/R26^{tdTomato}, and *RDX*$^{-/-}$ mice are provided in the Supplemental Experimental Procedures.

Immunofluorescent Stainings and Tracing Experiments

Immunofluorescent (IF) stainings, PLA for detection of in situ protein interaction, and anterograde and retrograde tracing experiments were performed following standard protocols.

Slice Culture Preparation, Biocytin Labeling, and Slice Electroporation

Organotypic slices were prepared as described in the Supplemental Experimental Procedures. For biocytin tracing experiments, pressure injections were performed into E17 embryonic slices using glass capillaries attached to a Toohey Spritzer (Toohey Company) to induce biocytin Alexa Fluor 488 (Thermo Fisher Scientific). Slices were then incubated for 6 hr and fixed with 4°C PFA (4%). For electroporation experiments, corresponding plasmids were injected into organotypic slices from E15.5 brains that were electroporated by Needle Tungsten Electrodes and an NEPA21 Super Electroporator (Nepa Gene).

Assessment of pERM Levels in Cortical Neurons

Cortical neurons were prepared as described (Vogt et al., 2012), cultivated for 2 days in vitro (DIV) and used for assessment of pERM levels in the GC. IF staining and pERM assessment were performed as described in the Supplemental Experimental Procedures.

IP Studies

IP studies were performed on E17 brain material or on cell lysate from stably PRG-2-expressing HEK293 cells according to standard protocols.

Intrinsic Signal Optical Imaging and In Vivo Electrophysiological Recordings

Intrinsic signal optical imaging (IOI) and in vivo electrophysiological recordings in the barrel cortex of adult mice were performed according to standard protocols as described in the Supplemental Experimental Procedures.

Animal Behavior

Sandpaper discrimination test and MWM were performed according to standard procedures.

Statistical Analysis

For animal experiments, mice from the same litter or of similar age were chosen. The investigator was blinded to the genotype of the animals. Following experiments, results were analyzed, animals were re-genotyped, and corresponding final statistical analyses were performed. Briefly, after assessing for normal distribution (using the Kolmogorov-Smirnov test), comparison between two groups, if not otherwise stated, was performed using a two-tailed unpaired t test for normal distributed data or a Mann-Whitney test for nonparametric data. When data were normalized to controls (set as 100%), a one-sample t test was used. For quantitative assessment of aberrant fibers in traced or electroporated slices, a Fisher's exact test was applied. p value was adjusted for multiple comparisons. Comparison between more than two groups was performed using a one-way ANOVA for parametric data or a Kruskal-Wallis

test for nonparamatric data. Variance was similar between groups and was estimated using either the F-test or the Brown-Forsythe test and Bartlett's test. Post hoc analysis for more than two groups for parametric data was performed using the Bonferroni adjustment for multiple comparisons and Dunn's test for nonparametric data. For behavioral analyses assessing genotype effects and time effects, as well as for comparisons of the multiple binding sites of PRG-2, a two-way ANOVA was used. Statistical analyses of data were performed using GraphPad Prism 5/6 or SPSS.

SUPPLEMENTAL INFORMATION

Supplemental Information includes Supplemental Experimental Procedures, eight figures, one table, and two movies and can be found with this article online at http://dx.doi.org/10.1016/j.neuron.2016.08.035.

AUTHOR CONTRIBUTIONS

Conceptualization, J.V. and R.N.; Methodology, J.V., J.C., K.R., and A.S.; Investigation, J.C., S.S., T.J.H., J.-W.Y., H.E., X.L., Y.L., R.B., H.J., N.S., H.M.M., A.H.-S., P.-H.P., W.F., and T.T.; B.V. and R.S. provided reagents; Writing – Original Draft, J.V.; Review and Editing, J.V., R.N., J.C., T.J.H., O.N., Z.M., H.J.L., and M.K.; Supervision, J.V., R.N., A.S., H.J.L., J.H., Z.M., K.S., M.K., and W.F.; Funding Acquisition, J.V., R.N., H.J.L., A.S., and M.K.

ACKNOWLEDGMENTS

We thank Darragh O'Neill for proofreading the manuscript and Melanie Pfeifer and Silke Fregin for technical assistance. We further thank Tineke Vogelaar for help with thalamus outgrowth assays and Menno P. Witter for help with retrograde tracings. Data from this study are part of the PhD theses of J.C. and S.S., and of the doctoral thesis of R.B. This work was supported by the Deutsche Forschungsgemeinschaft (SFB 1080) to J.V., R.N., A.S., and H.J.L., and the European Research Council (ERC-AG "LiPsyD" to R.N.). R.N. and J.V. contributed equally to this work.

Received: December 17, 2015
Revised: June 15, 2016
Accepted: August 16, 2016
Published: September 15, 2016

REFERENCES

Agmon, A., Yang, L.T., Jones, E.G., and O'Dowd, D.K. (1995). Topological precision in the thalamic projection to neonatal mouse barrel cortex. J. Neurosci. *15*, 549–561.

Birgbauer, E., and Chun, J. (2010). Lysophospholipid receptors LPA1-3 are not required for the inhibitory effects of LPA on mouse retinal growth cones. Eye Brain *2*, 1–13.

Bräuer, A.U., Savaskan, N.E., Kühn, H., Prehn, S., Ninnemann, O., and Nitsch, R. (2003). A new phospholipid phosphatase, PRG-1, is involved in axon growth and regenerative sprouting. Nat. Neurosci. *6*, 572–578.

Campbell, D.S., and Holt, C.E. (2003). Apoptotic pathway and MAPKs differentially regulate chemotropic responses of retinal growth cones. Neuron *37*, 939–952.

Chen, L., Guo, Q., and Li, J.Y. (2009). Transcription factor Gbx2 acts cell-non-autonomously to regulate the formation of lineage-restriction boundaries of the thalamus. Development *136*, 1317–1326.

Contos, J.J., Ishii, I., Fukushima, N., Kingsbury, M.A., Ye, X., Kawamura, S., Brown, J.H., and Chun, J. (2002). Characterization of lpa(2) (Edg4) and lpa(1)/lpa(2) (Edg2/Edg4) lysophosphatidic acid receptor knockout mice: signaling deficits without obvious phenotypic abnormality attributable to lpa(2). Mol. Cell. Biol. *22*, 6921–6929.

Cossell, L., Iacaruso, M.F., Muir, D.R., Houlton, R., Sader, E.N., Ko, H., Hofer, S.B., and Mrsic-Flogel, T.D. (2015). Functional organization of excitatory synaptic strength in primary visual cortex. Nature *518*, 399–403.

Fehon, R.G., McClatchey, A.I., and Bretscher, A. (2010). Organizing the cell cortex: the role of ERM proteins. Nat. Rev. Mol. Cell Biol. *11*, 276–287.

Fincher, J., Whiteneck, C., and Birgbauer, E. (2014). G-protein-coupled receptor cell signaling pathways mediating embryonic chick retinal growth cone collapse induced by lysophosphatidic acid and sphingosine-1-phosphate. Dev. Neurosci. *36*, 443–453.

Fukushima, N., Weiner, J.A., and Chun, J. (2000). Lysophosphatidic acid (LPA) is a novel extracellular regulator of cortical neuroblast morphology. Dev. Biol. *228*, 6–18.

Garion, L., Dubin, U., Rubin, Y., Khateb, M., Schiller, Y., Azouz, R., and Schiller, J. (2014). Texture coarseness responsive neurons and their mapping in layer 2-3 of the rat barrel cortex in vivo. eLife *3*, e03405.

Ghosh, A., Antonini, A., McConnell, S.K., and Shatz, C.J. (1990). Requirement for subplate neurons in the formation of thalamocortical connections. Nature *347*, 179–181.

Gierse, J., Thorarensen, A., Beltey, K., Bradshaw-Pierce, E., Cortes-Burgos, L., Hall, T., Johnston, A., Murphy, M., Nemirovskiy, O., Ogawa, S., et al. (2010). A novel autotaxin inhibitor reduces lysophosphatidic acid levels in plasma and the site of inflammation. J. Pharmacol. Exp. Ther. *334*, 310–317.

Guy, J., Wagener, R.J., Möck, M., and Staiger, J.F. (2015). Persistence of functional sensory maps in the absence of cortical layers in the somsatosensory cortex of reeler mice. Cereb. Cortex *25*, 2517–2528.

Hausrat, T.J., Muhia, M., Gerrow, K., Thomas, P., Hirdes, W., Tsukita, S., Heisler, F.F., Herich, L., Dubroqua, S., Breiden, P., et al. (2015). Radixin regulates synaptic GABAA receptor density and is essential for reversal learning and short-term memory. Nat. Commun. *6*, 6872.

Hoerder-Suabedissen, A., and Molnár, Z. (2015). Development, evolution and pathology of neocortical subplate neurons. Nat. Rev. Neurosci. *16*, 133–146.

Hoerder-Suabedissen, A., Oeschger, F.M., Krishnan, M.L., Belgard, T.G., Wang, W.Z., Lee, S., Webber, C., Petretto, E., Edwards, A.D., and Molnár, Z. (2013). Expression profiling of mouse subplate reveals a dynamic gene network and disease association with autism and schizophrenia. Proc. Natl. Acad. Sci. USA *110*, 3555–3560.

Kingsbury, M.A., Rehen, S.K., Contos, J.J., Higgins, C.M., and Chun, J. (2003). Non-proliferative effects of lysophosphatidic acid enhance cortical growth and folding. Nat. Neurosci. *6*, 1292–1299.

Kostovic, I., and Rakic, P. (1990). Developmental history of the transient subplate zone in the visual and somatosensory cortex of the macaque monkey and human brain. J. Comp. Neurol. *297*, 441–470.

Lokmane, L., Proville, R., Narboux-Nême, N., Györy, I., Keita, M., Mailhes, C., Léna, C., Gaspar, P., Grosschedl, R., and Garel, S. (2013). Sensory map transfer to the neocortex relies on pretarget ordering of thalamic axons. Curr. Biol. *23*, 810–816.

Madisen, L., Zwingman, T.A., Sunkin, S.M., Oh, S.W., Zariwala, H.A., Gu, H., Ng, L.L., Palmiter, R.D., Hawrylycz, M.J., Jones, A.R., et al. (2010). A robust and high-throughput Cre reporting and characterization system for the whole mouse brain. Nat. Neurosci. *13*, 133–140.

McDermott, M.I., Sigal, Y.J., Sciorra, V.A., and Morris, A.J. (2004). Is PRG-1 a new lipid phosphatase? Nat. Neurosci. *7*, 789.

Meyer, H.S., Wimmer, V.C., Hemberger, M., Bruno, R.M., de Kock, C.P., Frick, A., Sakmann, B., and Helmstaedter, M. (2010). Cell type-specific thalamic innervation in a column of rat vibrissal cortex. Cereb. Cortex *20*, 2287–2303.

Mintz, C.D., Carcea, I., McNickle, D.G., Dickson, T.C., Ge, Y., Salton, S.R., and Benson, D.L. (2008). ERM proteins regulate growth cone responses to Sema3A. J. Comp. Neurol. *510*, 351–366.

Molnár, Z., Adams, R., and Blakemore, C. (1998). Mechanisms underlying the early establishment of thalamocortical connections in the rat. J. Neurosci. *18*, 5723–5745.

Molnár, Z., Garel, S., López-Bendito, G., Maness, P., and Price, D.J. (2012). Mechanisms controlling the guidance of thalamocortical axons through the embryonic forebrain. Eur. J. Neurosci. *35*, 1573–1585.

Normand, E.A., Crandall, S.R., Thorn, C.A., Murphy, E.M., Voelcker, B., Browning, C., Machan, J.T., Moore, C.I., Connors, B.W., and Zervas, M. (2013).

Temporal and mosaic Tsc1 deletion in the developing thalamus disrupts thalamocortical circuitry, neural function, and behavior. Neuron *78*, 895–909.

Rhett, J.M., Jourdan, J., and Gourdie, R.G. (2011). Connexin 43 connexon to gap junction transition is regulated by zonula occludens-1. Mol. Biol. Cell *22*, 1516–1528.

Robichaux, M.A., Chenaux, G., Ho, H.Y., Soskis, M.J., Dravis, C., Kwan, K.Y., Šestan, N., Greenberg, M.E., Henkemeyer, M., and Cowan, C.W. (2014). EphB receptor forward signaling regulates area-specific reciprocal thalamic and cortical axon pathfinding. Proc. Natl. Acad. Sci. USA *111*, 2188–2193.

Trimbuch, T., Beed, P., Vogt, J., Schuchmann, S., Maier, N., Kintscher, M., Breustedt, J., Schuelke, M., Streu, N., Kieselmann, O., et al. (2009). Synaptic PRG-1 modulates excitatory transmission via lipid phosphate-mediated signaling. Cell *138*, 1222–1235.

Vogt, J., Glumm, R., Schlüter, L., Schmitz, D., Rost, B.R., Streu, N., Rister, B., Suman Bharathi, B., Gagiannis, D., Hildebrandt, H., et al. (2012). Homeostatic regulation of NCAM polysialylation is critical for correct synaptic targeting. Cell. Mol. Life Sci. *69*, 1179–1191.

Vogt, J., Yang, J.W., Mobascher, A., Cheng, J., Li, Y., Liu, X., Baumgart, J., Thalman, C., Kirischuk, S., Unichenko, P., et al. (2015). Molecular cause and functional impact of altered synaptic lipid signaling due to a prg-1 gene SNP. EMBO Mol. Med. *8*, 25–38.

Wagener, R.J., Witte, M., Guy, J., Mingo-Moreno, N., Kugler, S., and Staiger, J.F. (2016). Thalamocortical connections drive intracortical activation of functional columns in the mislaminated reeler somatosensory cortex. Cereb. Cortex *26*, 820–837.

Woolsey, T.A., and Van der Loos, H. (1970). The structural organization of layer IV in the somatosensory region (SI) of mouse cerebral cortex. The description of a cortical field composed of discrete cytoarchitectonic units. Brain Res. *17*, 205–242.